Fourth International Symposium on Marine Propulsors
smp'15, Austin, Texas, USA, June 2015

Numerical Simulation of Ship Hull Pressure Fluctuation Induced by Cavitation on Propeller with Capturing the Tip Vortex

Keita Fujiyama[1]

[1] Software Engineering Department,
Software Cradle Co., Ltd., Osaka, JAPAN

ABSTRACT

For the designing of ship and propeller, the interaction of them caused by cavitation is a very important factor and the preliminary study is needed to explain phenomena for the development. However, the experiment in the laboratory is expensive and requires substantial time, which sometimes makes the experiment difficult. Therefore, Computational fluid dynamics (CFD) is expected to be an effective tool to solve the problem in this field. This paper presents the calculations of ship hull pressure fluctuation induced by cavitation and the comparison of obtained calculation results with the experimental data of the previous study. It also explains the relationship between the pressure fluctuation components and the cavitation phenomena. Finally, we evaluated the accuracy and the potential of CFD for the ship and propeller designing.

Keywords

Numerical Simulation, Cavitation, Pressure Fluctuation, Tip Vortex

1 INTRODUCTION

The construction of ships has encountered some environmental problems such as the greenhouse gas emissions and the noise on marine life, and sought the solutions including higher fuel efficiency of ships. To build a "high-performance ship", developers must prepare many development plans in the design phase, then, review and choose the best one from them. However, conducting experiments for all the plans costs huge and takes an immense amount of time. For this reason, experiments are done basically only for the final design. Therefore, the importance of numerical simulations as helpful tools for the designing process of ships is growing to overcome the experimental difficulties.

The interaction between the wake of a ship and the rotation of its propeller causes unsteady cavitation. The cavitation causes the pressure fluctuation on a ship, which affects both comfort on board and the fatigue strength of the ship structure. In addition, there is a possibility that the noise caused by the cavitation attacks the sea animals. To protect them, the noise must be controlled and the regulation is now being prepared. For these reasons, predicting unsteady cavitation and pressure fluctuation on a ship hull in the design phase is essential for developing ships.

The studies of the propeller cavitation in the wake of a ship and the pressure fluctuation on a ship hull, using the numerical simulations, have been presented by Kanemaru et al. (2013) and Berger et al. (2013). Kanemaru et al. used the extended panel method while Berger et al. used the finite element method around the ship hull and the boundary element method for the propeller in combination. Moreover, Hasuike et al. (2011) and Sato et al. (2009) simulated unsteady propeller-cavitation using CFD based on the finite element method or the finite volume method. They applied a non-uniform inflow condition with the distribution of the wake to the calculation. On the other hand, Kawamura et al. (2010) and Paik et al. (2013) simultaneously analyzed both the ship hull and the propeller to calculate the cavitation. In all these studies, the results show that the first component of the blade passing frequency of the pressure fluctuation can be predicted with a certain level of accuracy. However, the amplitude of higher-level components of the frequency is not predicted well. Konno et al. (2002) suggested that the higher-level components of the frequency of the pressure fluctuation are affected by collapse of the tip vortex cavitation; however, there were less consideration for the tip vortex cavitation in the aforementioned calculations.

In this paper, we used a model of a ship and its propeller in combination to perform numerical simulations of unsteady cavitation including the tip vortex cavitation. Then, we compared the numerical results with the experimental results presented by Kurobe et al. (1983) to examine the relationships between the cavitation phenomena and the pressure fluctuation on a ship hull. Lastly, we evaluated the accuracy and the potential of CFD software as a cavitation prediction tool used in design and development of ship hulls and propellers.

2 NUMERICAL METHOD

All simulations in this paper were performed by the SC/Tetra Version 11, which is the commercial navier-stokes solver based on a finite volume method. In these calculations, the combination of the compressibility two phase one fluid model by Okuda et al. (1996) and the full cavitation model by Singhal et al. (2002) was used as the cavitation calculation method, and the SST-SAS model was used as the turbulence model which is the effective method for the transient cavitation analysis reported by our previous paper (2012).

2.1 Cavitation Model

In this paper, relative motions between vapour and liquid are neglected since the flows are assumed to be uniform. In addition, a barotropic relation is used and the governing equations of mass and momentum are formally the same as those of the single phase flows.

Mixture density is described as follows:

$$\rho = \sum \alpha_N \rho_N \tag{1}$$

where, N denotes phase and α volume fraction. By using this mixture density, mass and momentum conservation equations are described as follows:

$$\frac{\partial \rho}{\partial t} + \frac{\partial \rho u_i}{\partial x_i} = 0 \tag{2}$$

$$\frac{\partial \rho u_i}{\partial t} + \frac{\partial \rho u_i u_j}{\partial x_j} = -\frac{\partial P}{\partial x_i} + \frac{\partial \tau}{\partial x_j} \tag{3}$$

where, τ indicates shear stress.

Cavitating flows are applied as compressible flows. Thus the barotropic relation is employed to the equation of the state. Mixture density containing a non-condensable gas can be specified by mass fraction instead of volume fraction.

$$\frac{1}{\rho} = \frac{Y_v}{\rho_v} + \frac{Y_g}{\rho_g} + \frac{1 - Y_v - Y_g}{\rho_l} \tag{4}$$

where, Y_v and Y_g denote mass fraction of vapour and a non-condensable gas, respectively. Mass fraction of a non-condensable gas is assumed to be constant analysis parameter. Density of the non-condensable gas is obtained by the following equation.

$$\rho_g = \frac{P}{RT} \tag{5}$$

where, R is a gas constant of the non-condensable gas and the flow field is assumed to be isothermal because temperature T is also a constant.

Mass fraction of vapour is calculated by the transport equation below.

$$\frac{\partial \rho Y_v}{\partial t} + \frac{\partial \rho u_i Y_v}{\partial x_i} = R_e - R_c \tag{6}$$

The right-hand side is source terms indicating evaporation and condensation which are modelled by the full-cavitation model by Singhal et al (2002).

$$R_e = C_e \frac{\sqrt{k}}{\sigma} \rho_l \rho_v \sqrt{\frac{2}{3}\frac{P_v - P}{\rho_l}} \left(1 - Y_v - Y_g\right) \tag{7}$$

$$R_c = C_c \frac{\sqrt{k}}{\sigma} \rho_l \rho_l \sqrt{\frac{2}{3}\frac{P - P_v}{\rho_l}} Y_v \tag{8}$$

where, k denotes turbulent kinetic energy, ρ_l and ρ_v density of liquid and vapor, respectively, and surface tension coefficient. In the full cavitation model, the effect of turbulence is taken into account for the threshold of pressure P_v, where evaporation occurs.

$$P_v = P_s + \frac{0.39\rho k}{2} \tag{9}$$

where, P_s indicates the saturation pressure. The model constants are $C_e = 0.02$ and $C_c = 0.01$.

2.2 SST-SAS Turbulence Model

The SST k-ω model developed by Menter (1993) solves the two equations for k and ω with a zonal treatment the conventional k-ω equations developed are solved in near-wall regions, and they are shifted toward outer regions to be equivalent to the k-ε model, which promises an accurate and robust computation. Also, the concept of Shear-Stress Transport avoids the over-estimate of eddy viscosity under adverse pressure-gradients, and properly reproduces complicated separation phenomena that the conventional eddy viscosity models may fail to capture.

The SST model is suitable for the analysis of flow with separation phenomena. However, as a general feature of RANS models, to reproduce unsteady flow in the separation zone are difficult. SST-SAS (Scale-Adaptive Simulation) model by Egorov et al. (2008) is which is derived from the SST model is proposed to solve the problem. The model reduces its eddy viscosity depending on the local length scale of the turbulent flow, and this brings the similar results as that obtained by using RANS/LES hybrid models such as DES. Specifically, the following additional source term Q_{SAS} is added in the transport equation of ω to control the production of the turbulence energy:

$$Q_{SAS} = max\left[\rho \eta_2 \kappa S^2 \left(\frac{L}{L_{vk}}\right)^2 - C\frac{2\rho k}{\sigma_\Phi} max\left(\frac{|\nabla \omega|^2}{\omega^2}, \frac{|\nabla k|^2}{k^2}\right), 0\right] \tag{10}$$

The value L in the above equation (10) is the modeled length scale on the assumption of homogeneous turbulent flow, and the L_{vk} (von Karman length scale) is the length

scale which is derived from the velocity gradients to indicate inhomogeneous nature of the turbulent flow. Those are defined as follows:

$$L = \sqrt{k} \Big/ \left(C_\mu^{\frac{1}{4}} \cdot \omega \right) \tag{11}$$

$$L_{vk} = max \left[\frac{\kappa S}{|\nabla^2 U|}, C_s \sqrt{\kappa \eta_2 \Big/ \left(\frac{\beta}{C_\mu} - \alpha \right)} \cdot \Delta \right] \tag{12}$$

3 ANALYSIS CONDITIONS

3.1 Calculation Model Setup

All of the calculation setups are according to the experiments conducted by Kurobe et al. (1983). Figure 1 shows the actual calculation region, which is the same size as the large cavitation tunnel in NMRI (National Maritime Research Institute in JAPAN). In the experiments, auxiliary equipment called Flow Liner was installed to make the velocity distribution of the model ship wake closer to the real one. Therefore, the equipment was modeled in the calculation to make it closer to the experiments.

The specifications of the ship are shown in Table 1 and twelve points for pressure measurement are set on the surface of the ship hull as shown in Figure 2. Figure 3 shows two types of propellers used in the calculation, i.e., HSP-II and CP-II, whose specifications are listed in Table 2.

3.1 Calculation Conditions

The mesh specifications for the calculation are listed in Table 3 and Figure 4 shows the elements around the propeller. The calculation mesh is characterized with the fine elements around the tip vortex region which are generated by using automated adaptive meshing. For specific steps: 1. run a steady-state analysis of ship in the behind-hull condition with coarse mesh, 2. use the result to automatically generate finer mesh, actually required for cavitation analysis, at the tip vortex region.

The propeller operating conditions are listed in Table 4. In ship-cavitation-related experiments, the thrust coefficient $K_T = T/0.5pn^2D^4$ (T: Thrust [N]) is adjusted to be a predefined value by changing the inflow speed. Therefore, in this calculation, an incompressible steady-state analysis with non-cavitation was performed first and the inflow velocity is adjusted so that K_T is to be a predefined value. Then, unsteady cavitation analyses were executed by using the adjusted inflow boundary conditions. It was confirmed in advance that there are almost no differences of the K_T values between calculations with non-cavitation and cavitation conditions.

4 RESULTS AND DISCUSSION

4.1 Wake Distribution behind hull

Figure 5 shows the comparison of wake distributions between the experiment and the calculation. The distributions are measured or calculated on the propeller

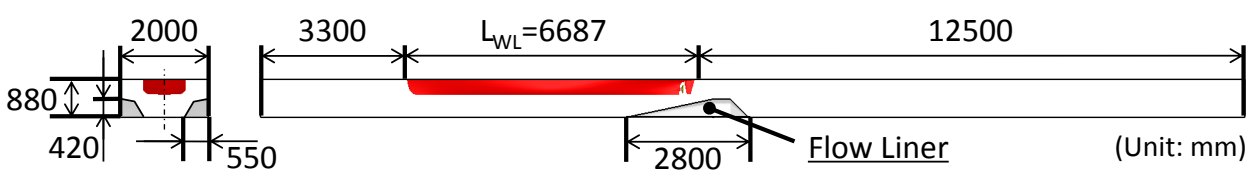

Figure 1: Computational domain.

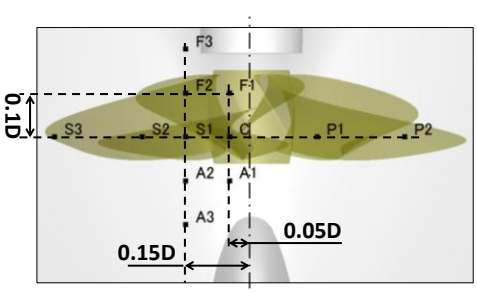

Figure 2: Location of pressure measurement points.

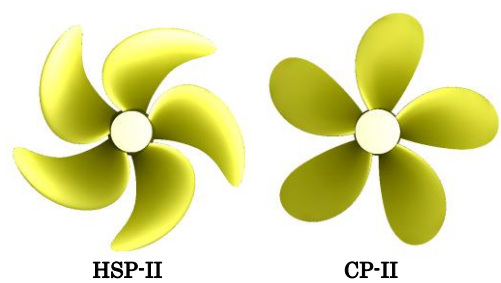

Figure 3: Overviews of testing propellers.

Table 1: Model description.

Ship Name	Seiunmaru(I)
Scale	1/16.293
L_{WL}	6687 mm

Table 2: Propeller descriptions.

Propeller Name	HSP-II	CP-II
Diameter	220 mm	221 mm
Number of Blade	5	5

Table 3: Mesh descriptions.

Element Type	Tetra + Prism
Number of Elements	30,000,000
Number of Nodes	6,000,000

Table 4: Testing conditions.

Propeller Name	HSP-II	CP-II
K_T	0.201	0.207
σ_n	2.99	3.06
Revolution	17.5 rps	17.15 rps

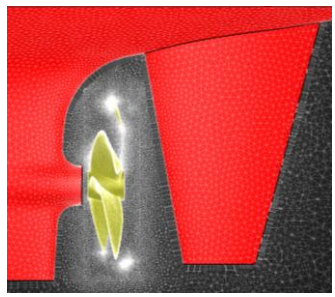

Figure 4: Computation mesh around propeller.

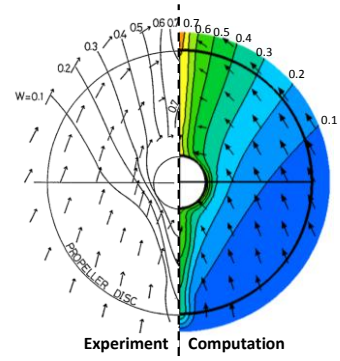

Figure 5: Comparison of the wake distributions between the results from experiment and calculation.

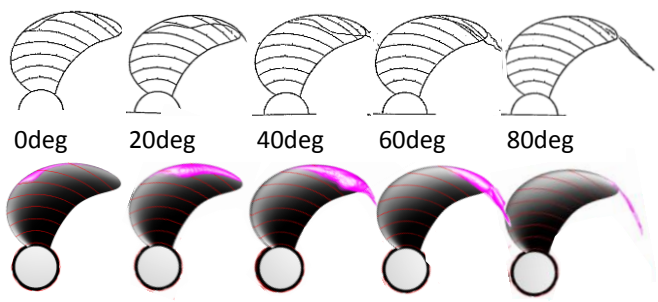

Figure 6: Comparisons of the HSP-II propeller cavitation patterns between the results from experiment and calculation.

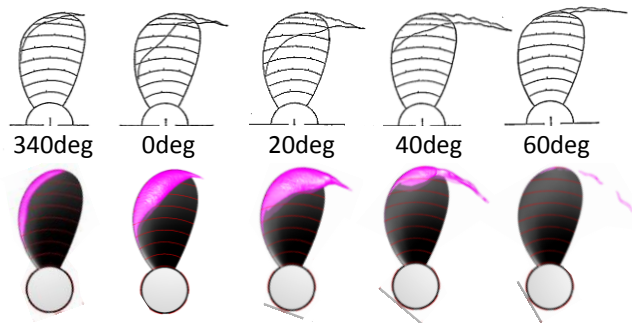

Figure 7: Comparisons of the CP-II propeller cavitation patterns between the results from experiment and calculation.

disk plane when the propeller was uninstalled. This result shows that the thinning of the slow-velocity region which may be caused by bilge vortices on the ship side was not simulated well in the lower part of the propeller disc plane. On the other hand, the velocity distribution was well simulated in the upper part of the propeller, which is an important region for the cavitation. Then, it is considered that the cavitation analyses afterward can be done well.

4.2 Cavitation Behavior

Figure 6 and Figure 7 show the comparisons of the cavitation pattern between the sketch from the experiments and the isosurface of 10% void fraction from the calculations for each propeller. These results show that the cavitation patterns of both CP-II and HSP-II propellers are basically the same.

The comparison of the cavitation volume between the experiments and the calculations is shown in Figure 8. Note that the experimental result was obtained by using sheet cavitation measurement with the laser and does not contain the tip vortex cavitation volume, although the volume is contained in the calculation results. The comparison result of the volume shows that the calculation results of CP-II propeller well agree with the experiments. However, the predictions of the HSP-II propeller have a few underestimates of the cavitation volume and a little delay in the cavitation phase, which have not been found from the sketch.

4.3 Ship Hull Pressure Fluctuations

Figure 9 shows the raw pressure waveform at the point C located just above the propeller. FFT was performed by using the profiles and the amplitude coefficient of the pressure fluctuation, $K_{pi} = \Delta P_i / \rho n^2 D^2$; where P_i is the i-th harmonic component of propeller rotation frequency of fluctuation pressure waveform, was compared between the experiments and the calculations. Figure 10 shows the amplitude distribution of the first component of blade passing frequency, K_{p5}, for each position and each propeller. These results show that the difference of the amplitude between two propellers is well simulated especially in the transversal direction. On the other hand, the accuracy in the longitudinal direction is not enough.

Next, the amplitude distribution of the second component of blade passing frequency, K_{p10}, was compared as shown in Figure 11. These results show that the amplitude of CP-II propeller well agrees with that measured in the experiments. However, the results of HSP-II show lower level of agreement than the CP-II. This difference may be due to the underestimates of the cavitation volume explained in section 4-2.

Finally, the amplitude of the first to the fourth components of the blade passing frequency at the point C was compared

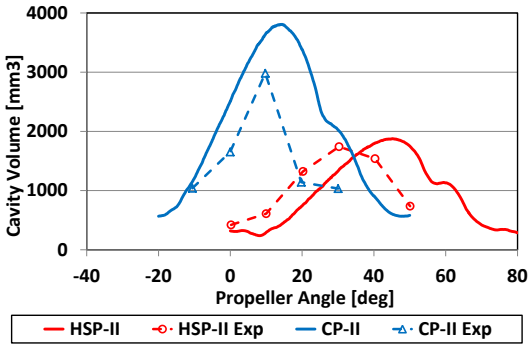

Figure 8: Comparisons of the cavitation volumes between the results from experiment and calculation.

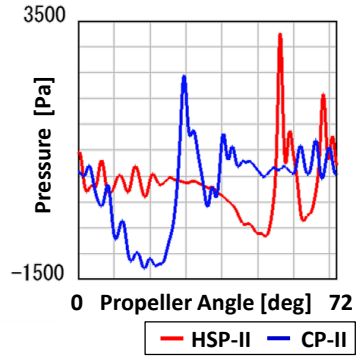

Figure 9: The pressure fluctuation waveforms by the calculation at the point C.

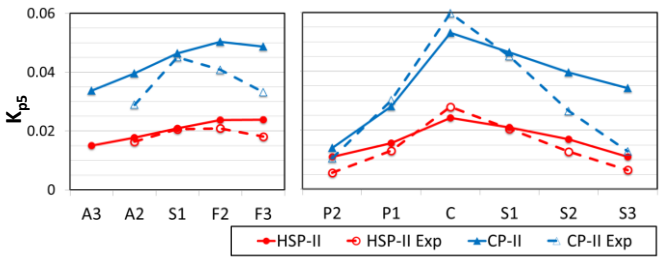

Figure 10: Amplitude distributions of pressure fluctuation. (1st blade frequency component)

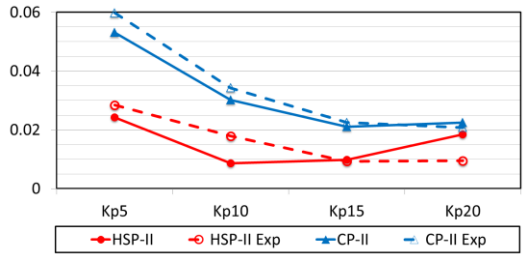

Figure 12: Amplitude of pressure fluctuation at Point C.

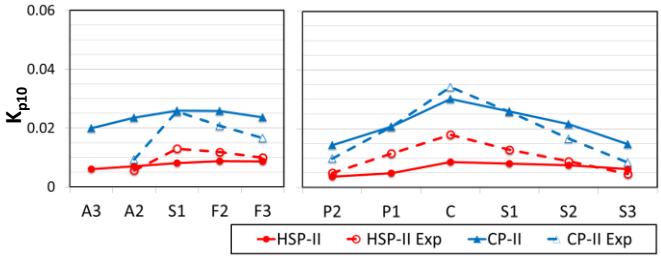

Figure 11: Amplitude distributions of pressure fluctuation. (2nd blade frequency component)

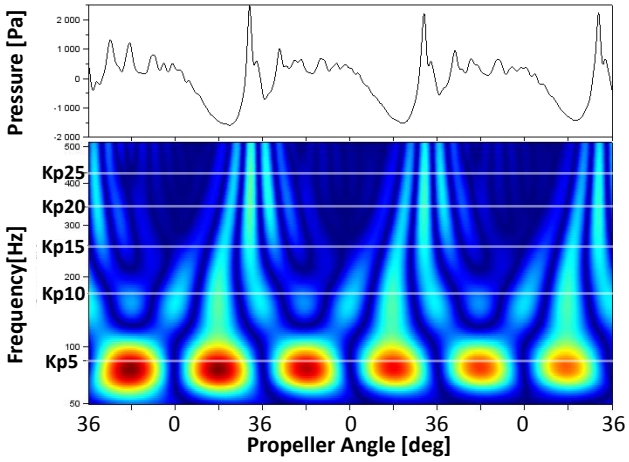

Figure 13: The result of discrete wavelet transform of pressure fluctuation on CP-II propeller at Point C.

as shown in Figure 12. The calculation results agree with the experimental results for all the components in a certain level, rather well for those of CP-II propellers. Therefore, these results show that the calculation method can be used to predict the wide range of frequency components of the hull pressure fluctuation with high accuracy.

4.4 Wavelet Analysis of Pressure Fluctuations

To clarify the relationship between cavitation and pressure fluctuation on the ship hull in detail, a discrete wavelet transform was applied to the waveform of the pressure fluctuation. A discrete wavelet transform is a method to obtain amplitude information with the temporal resolution in wider range of frequency than FFT. In this paper, Gabor Wavelet, written in Eq. (13), was employed as the mother wavelet for the transform.

$$\psi(t) = \frac{1}{\sqrt{2\pi\sigma^2}} e^{-t^2/2\sigma^2} e^{i\omega t} \tag{13}$$

where ω is the angular rate corresponding to the frequency, and σ is a parameter which affect the frequency resolution. In this paper, $\sigma = 8$ was used.

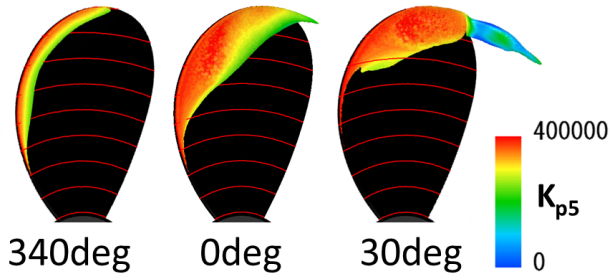

Figure 14: Distributions of K_{p5} component on the 10% void fraction isosurface.

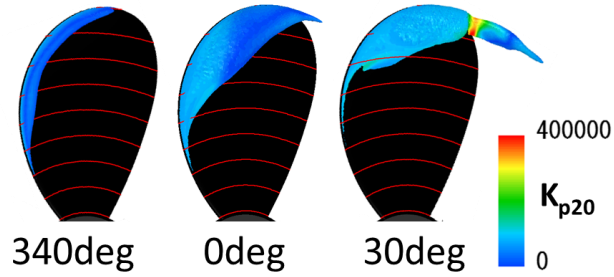

Figure 15: Distributions of K_{p20} component on the 10% void fraction isosurface.

Figure 13 shows the result of a discrete wavelet transform at point C during the operation of CP-II propeller. In this graph, the vertical axis indicates frequency component while horizontal axis time. In this result, high level amplitude regions such as K_{p20} (4th component) and K_{p25} (5th component) are around the propeller angle of 30 degrees. The regions are different from the region formed from K_{p5}.

To explain the state of cavitation which induces these higher level components, the distributions of K_{p5} and K_{p20} were drawn on the isosurface of the 10% void fraction (Figure 14 and Figure 15). As shown in the figures, K_{p5} component is mainly caused by generation and collapse of the sheet cavitation on the propeller surface.

As for K_{p20}, the main factor is the collapse of the tip vortex cavitation around the propeller angle of 30 degrees. The results match the study suggested by the Konno et al. (2002) that the higher components of pressure fluctuation are caused by tip vortex cavitation bursting. In addition, it is proved that a discrete wavelet transform is useful for factorial analyses of the pressure fluctuation on the ship hull.

5 CONCLUSIONS

The computational fluid analysis of the cavitation on the propeller in the behind-hull condition was performed. From the calculation result, unsteady cavitation and the pressure fluctuation induced by the cavitation were evaluated, and the following conclusions were obtained.

1) The simulation using CFD software achieves high accuracy in prediction of the cavitation which occurs on the blade surface and at the tip vortex region.

2) Because the CFD software well simulated unsteady cavitation with high accuracy, wide range of component-level of pressure fluctuation on a ship hull induced by the cavitation was well calculated. This means that the calculation using CFD software is an effective tool for ship designing.

3) A discrete wavelet analysis of the calculated pressure pulse showed that the tip vortex cavitation causes the high-frequency component of pressure fluctuation. By using this analysis method, the relationship between cavitation and pressure fluctuation can be visualized, which will be applied to more advanced design and development.

REFERENCES

Berger, S., Bauer, M., Druckenbrod, M., and Abdel-Maksoud, M., (2013), “Investigation of Scale Effects on Propeller-Induced Pressure Fluctuations by a Viscous/Inviscid Coupling Approach”, Proc. Third International Symposium on Marine Propulsors

Egorov, Y., and Menter, F., (2008), “Development and Application of SST-SAS Turbulence Model in DESIDER Project”, Advances in Hybrid RANS-LES Modelling, 261-270

Fujiyama, K., Kim, J-H., Hitomi, D., and Irie, T., (2012), “Numerical Analysis of Unsteady Cavitation Phenomena by using RANS Based Methods (in Japanese)”, Proc. the 16th Cavitation Symposium

Hasuike, N., Yamasaki, S., and Ando, J., (2011), “Numerical and Experimental Investigation into Propulsion and Cavitation Performance of Marine Propeller”, Proc. the 4th International Conference on Computational Methods in Marine Engineering

Kanemaru, T., and Ando, J., (2013), “Numerical analysis of cavitating propeller and pressure fluctuation on ship stern using a simple surface panel method “SQCM”, Journal of Marine Science and Technology, 18(3), 294-309

Kawamura, T., (2010), “Numerical Simulation of Propulsion and Cavitation Performance of Marine Propeller”, Proc. International Propulsion Symposium

Konno, A., Wakabayashi, K., Yamaguchi, H., Maeda, M., Ishii, N., Soejima, S. and Kimura, K., (2002), “Generation Mechanism of Bursting Phenomena of Propeller Tip Vortex Cavitation”, Journal of Marine Science and Technology, 6(4), 181-192

Kurobe, Y., Ukon, Y., Koyama, K., and Makino, M., (1983), "Measurement of Cavity Volume and Pressure Fluctuation on a Model of the Training Ship 'SEIUNMARU' with Reference to Full Scale Measurement (in Japanese)", SRI Report, 20(6), 395-429

Menter, F., (1993), "Zonal Two Equation k-ω Turbulence Models for Aerodynamic Flows", AIAA 1993-2906

Okuda, K. and Ikohagi, T., (1996), "Numerical Simulation of Collapsing Behavior of Bubble Clouds (in Japanese)", Trans. of JSME(B), 62(603), 3792-3797

Paik, K. J., Park, H-G., and Seo, J., (2013), "URANS Simulations of Cavitation and Hull Pressure Fluctuation for Marine Propeller with Hull Interaction", Proc. Third International Symposium on Marine Propulsors

Sato, K., Ohshima, A., Egashira, H., and Takano, S., (2009), "Numerical Prediction of Cavitation and Pressure Fluctuation around Marine Propeller", Proc. the 7th International Symposium on Cavitation

Singhal A. K., Athavale, M. M., Li, H., and Jiang, Y., (2002) "Mathematical basis and validation of the full cavitation model", Journal of Fluids Eng., 124(3), 617-624

DISCUSSION

Question from Johan Bosschers

Thank you for your interesting presentation. This is one of the few papers where the higher harmonic pressure due to the collapse of cavitating tip vortex seems to be captured by CFD. I have one remark on the diagram with the wavelet transform: My experience is that the power in the signal is better represented if you take the absolute value of the wavelet coefficients of the Hilbert transform of the time series. My question is also related with wavelet diagram: how do these results compare to the results of the measurements?

Authors' Closure

Thank you for your observation. In this study, the amplitudes of pressure fluctuations were compared with the coefficients only by the FFT analyses, not by the wavelet analyses. It is because the results of both the wavelet coefficients and the raw waveform of pressure fluctuations were not provided from experiments. For the qualitative observation, this method is useful in its own way. However, to use it at quantitative analysis, the method needs to be improved and validated.